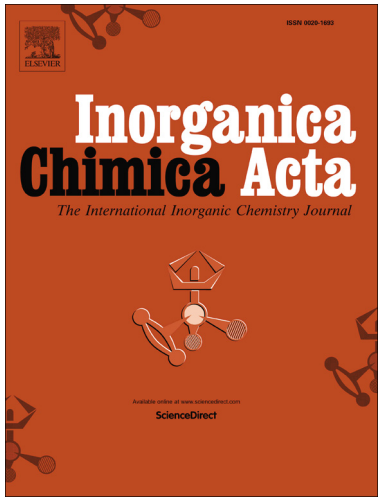

Research paper

Synthesis, Crystal structure and Biological studies of New Hydrazone ligand, 2-(Methoxycarbonyl-hydrazono)-pentanedioic acid and its Silver(I) complex

S. Parveen, S. Govindarajan, Horst Puschmann, R. Revathi

PII: S0020-1693(17)31497-4
DOI: https://doi.org/10.1016/j.ica.2018.02.022
Reference: ICA 18132

To appear in: *Inorganica Chimica Acta*

Received Date: 27 September 2017
Revised Date: 23 January 2018
Accepted Date: 17 February 2018

Please cite this article as: S. Parveen, S. Govindarajan, H. Puschmann, R. Revathi, Synthesis, Crystal structure and Biological studies of New Hydrazone ligand, 2-(Methoxycarbonyl-hydrazono)-pentanedioic acid and its Silver(I) complex, *Inorganica Chimica Acta* (2018), doi: https://doi.org/10.1016/j.ica.2018.02.022

Synthesis, Crystal structure and Biological studies of New Hydrazone ligand, 2-(Methoxycarbonyl-hydrazono)-pentanedioic acid and its Silver(I) complex

S.Parveen[a], S.Govindarajan[a*], Horst Puschmann[b] and R.Revathi[c]

[a]Department of Chemistry, Bharathiar University, Coimbatore-641046, Tamil Nadu, India
[b]Department of Chemistry, Durham University DH1 3LE, United Kingdom
[c]Department of science and Humanities, SRIT, Coimbatore-641010, Tamil Nadu, India
*Corresponding author: Email: drsgovind @yahoo.co.in
Telephone number: +91 9486036449

Abstract

A new hydrazone ligand (2-(Methoxycarbonyl-hydrazono)-pentanedioic acid, **H_2L**), derived from methyl carbazate and α-ketoglutaric acid, and its Ag(I) complex **[Ag(HL)(H_2L)]** were synthesised and characterised by elemental, spectral and thermal analyses. The X-ray structures of the ligand and complex were determined. The silver ion is hexa-coordinated to two tridentate (O, N, O) hydrazone ligands in a distorted octahedral environment. The binding carboxylic acid group is protonated in one of the ligands (netural) while it is present as the carboxylate in the other (negatively charged) ligand. The bulk material of the complex thermally decomposes to form metallic silver sheets. The ability to scavenge radical of both, the ligand and complex, was studied against these radicals: $DPPH^{\bullet}$, $ABTS^{\bullet+}$, $NO^{\bullet}$ and $O_2^{\bullet-}$. The binding affinity and mode of binding towards CT-DNA were recorded by UV-absorption and the ethidium bromide displacement method. The interaction of ligand and complex with bovine serum albumin was investigated using UV-Vis, fluorescence and synchronous spectroscopic methods. The silver complex showed strong binding propensity than the free Schiff base ligand in binding studies. The antimicrobial activity was studied against both bacteria and fungi strains and the silver complex exhibited significant activity as compared to the ligand alone. Significantly high antimicrobial activity was noticed especially for *Staphylococcus aureus,* and *Escherichia coli* which were extensively studied by MIC

methods. Furthermore, the ligand and complex show potential cytotoxicity towards the MCF-7 breast cancer cell line. Both of them have been found to induce apoptosis confirmed by AO/EtBr and DAPI staining assays.

Key words

Hydrazones; apoptosis staining; antimicrobial activity; DNA- and BSA- binding.

1. Introduction

Metal complexes containing methyl and ethyl carbazates (R-O-CO-NH-NH_2, R= -CH_3, -C_2H_5) have been of considerable interest due to their interesting thermal and structural properties [1-9]. Carbazates are interesting as ligands in view of their variety of potential oxygen and nitrogen donar atoms and these neutral molecules are expected to exhibit only one a common coordination mode, namely bidendate N, O- chelation. Apart from its coordination ability, alkyl carbazates can also undergo condensation reactions; the hydrazinic part of the terminal amine group reacts with the carbonyl groups of aldehydes or ketones to form Schiff bases. However, Schiff bases and their metal complexes derived from methyl and ethyl carbazate have not been studied except our own recent reports [10-13] of Schiff bases derived from analogous benzyl carbazate with alkyl and heteroaryl ketones and their metal complexes.

The ability of Schiff base complexes to interact with DNA and proteins has attracted much attention in the search for new chemotherapeutic agents and nucleic acid structural probes [14,15]. Also our recent study [11] has shown that the Schiff base complexes strongly bind to HSA, the essential distributors of metal ions, drugs and various metabolites throughout the human body [16]. Therefore, to obtain new pharmaceutically active compound is to combine different pharmacophore groups in the same molecule. In this context, α- Ketoglutaric acid is a naturally occurring ketoacid and an important intermediate in the Krebs cycle, which generates energy for life processes. Further, from the literature survey, it appears that the

work involving Schiff base complexes derived from α- Ketoglutaric acid and hydrazine derivatives was the reports on thiosemicarbazide [17] and substituted thiosemicarbazide [18].

Against this background we have examined the synthesis and characterisation of silver(I) complex of Schiff base ligand derived from methyl carbazate and α- Ketoglutaric acid, and studied their chemical and biological behaviour. Metal-based drugs exhibit more cytotoxic activity against cancer cells than their corresponding ligands. The present study describes the antimicrobial and cytotoxic activity of this silver (I) complex. The antioxidant activity and binding studies towards DNA, BSA have also been carried out and discussed herein.

2. Experimental

2.1. Material and methods

All reagents and chemicals used were of Analytical reagent grade (A.R) and of highest purity. Doubly distilled water was used as a solvent in all preparations and experiments. Calf thymus CT-DNA, Tris–Tris(hydroxymethyl)methylamine, Ethidium bromide (EB), were purchased from sigma. The stock solution of CT-DNA was prepared in 5 mM Tris HCl/50 mM NaCl at pH 7.2 and the ratio of absorbance at 260 & 280 nm above 1.8:1 indicating that the CT-DNA preparation was free from protein contaminations [19]. BSA stock was prepared by dissolving the BSA in 50 mM phosphate buffer at pH 7.4. All stock solutions were stored at 4˚C and used within two days. The Human breast cancer and normal breast epithelial cells were purchased from the National Centre for Cell Sciences (NCCS), Pune, India.

Elemental analysis for C, H, and N were performed on a Vario-ELIII elemental analyser. The IR spectra were recorded on a JASCO- 4100 spectrophotometer as KBr pellets in the range of 4000-400 cm^{-1}. Simultaneous TG-DTA studies were done on a Perkin – Elmer Pyris Diamond thermal analyser and the curves obtained in air using platinum cups as holders with 3 mg of the samples at the heating rate of 10˚C/min. Absorption spectral analysis were performed using JASCO V-630 UV-Visible spectrophotometer with quartz cuvettes of path

length 1cm. NMR spectra were recorded on a Breuker Avance III spectrometer operating at 400MHz for ^{1}H and 100 MHz for ^{13}C. $^{1}H/^{13}C$ NMR chemical shifts are reported in ppm and tetramethyl silane (TMS) used as an internal reference.

Crystal data were collected using a Xcalibur, Sapphire3 diffractometer (MITIGEN holder in perfluoroether oil) equipped with an Oxford Cryosystems 700 Plus Series low-temperature apparatus operating at T = 120(2)K. Data were measured ω scans of 1.0° per frame for 6.0 s using MoK_{α} radiation (Enhanced (Mo) X-ray Source, 50 kV, 35 mA). The total number of runs and images was based on the strategy calculation from the program CrysAlisPro (Agilent) [20]. Actually achieved resolution was Θ = 26.498(Ag) 32.844(L). Data reduction was performed using the CrysAlisPro (Agilent) software which corrects for Lorentz polarisation. The absorption coefficient (μ) of the ligand and complex are 0.139 & 1.134 and the minimum and maximum transmissions are 0.904 and 0.981 & 0.738 and 0.886 respectively. Using Olex2 the structure was solved with the olex2.solve structure solution program, in the Charge Flipping solution method [21,22]. The model was refined with version of SHELXL using Least Squares minimisation [23]. All non-hydrogen atoms were refined anisotropically. Hydrogen atom positions were calculated geometrically and refined using the riding model.

2.2. Synthesis

H_2L: Alpha ketoglutaric acid (0.146 g, 1 mmol) and methyl carbazate (0.092 g, 1 mmol) were dissolved in 20 mL of doubly distilled water and heated on a water bath for 4 h. The resulting clear solution was allowed to crystallize at room temperature. Block shaped colourless crystals formed after three days, were filtered off, washed with cold water followed by ethanol and air dried. Yield: 95%, Elemental analysis found: C, 35.68%; H, 5.20%; N, 11.58%. $C_7H_{12}N_2O_7$: Calc. C , 35.59%; H, 5.12%; N, 11.86%. UV-Vis (10^{-3} M, λ_{max}, nm (ε [$M^{-1}cm^{-1}$])): 240 (20450), 289 (17500). FT-IR (KBr, cm^{-1}): 3607, 3476 (OH), 3214 (NH), 1739 (C=O), 1602 (C=N), 1048 (N-N). ^{1}H NMR (400 MHz, DMSO-d6, δ, ppm):

10.73(s, NH), 3.73(s, OCH_3), 3.71(s, H_2O), 2.69-2.65(t, 7.4 Hz, CH_2), 2.38-2.34 (t, 7.6 Hz, CH_2). ^{13}C NMR (100 MHz, DMSO-d6): 173.48 (C7), 165.38 (C1), 154.09 (C3), 143.52 (C2), 52.41 (C4), 29.66 (C6), 21.06(C5).

[Ag(HL)(H_2L)]: To a hot aqueous solution (20 mL) of ligand (0.472 g, 2 mmol), 0.170 g of silver nitrate (1 mmol) dissolved in 20 mL of water was added in drops with continuous stirring, over water bath to prevent precipitation. Careful addition of aqueous solution of 3-4 drops of triethylamine was made to facilitate complexation. The resulting solution on evaporation at ambient condition resulted polycrystalline solid which was separated as before. The compound was stored in dark at all times. Glossy white crystals suitable for diffraction studies were obtained only at fifth time of crystallisation. Yield: 88%. Elemental analysis found: C, 30.70%; H, 3.01%; N, 10.41%. Ag, 19.70%; $C_{14}H_{19}AgN_4O_{12}$: Calc. C , 30.95%; H, 3.52%; N, 10.31%; Ag, 19.85%. UV-Vis (10^{-3} M, λ_{max}, nm (ε [$M^{-1}cm^{-1}$])): 242 (24800), 293 (18600). FT-IR (KBr, cm^{-1}): 3420 (OH), 3209 (NH), 1724 (C=O), 1585 (C=N) 1545, 1266 (COO^-), 1056 (N-N). ^{1}H NMR (400 MHz, DMSO-d6, δ, ppm): 8.30(s, NH), 3.74 (s, OCH_3), 3.65 (s, OCH_3), 2.74-2.70 (t, 7.8 Hz, CH_2), 2.60-2.57(t, 7.4 Hz, CH_2), 2.47-2.42 (t, 7.4 Hz, CH_2), 2.39-2.35 (t, 7.6Hz, CH_2). ^{13}C NMR (100 MHz, DMSO-d6):173.87 (C7), 165.31 (C1), 79.10 (C3 & C2), 52.45 (C4), 29.74 (C6), 21.26 (C5).

2.3. DNA binding studies

Ligand and complex were first dissolved in DMSO to give 1 mM stock solutions, which further diluted in 5 mM Tris HCl/50 mM NaCl buffer at pH 7.2. Electronic absorption spectra were recorded in the range of 200-500 nm by increasing concentration of CT-DNA (30 µM) to the complex (50 µM). The solution mixture was kept for 10 min at equilibrium before recording spectrum. Competitive EB binding study was performed in order to investigate that compounds could replace EB from EB-DNA system by fluorescence spectroscopic titration. The fluorescence emission spectra were recorded in the wavelength range of 530-700 nm, with excitation wavelength at 525 nm after successive addition of

compounds to a solution containing 8 µM EB and 10 µM CT-DNA.

2.4. Albumin binding studies

Binding studies with protein by tryptophan fluorescence quenching experiments were performed using Bovine Serum Albumin (BSA) as a model protein. Like DNA binding studies, compound's stock solutions were prepared by using 50 mM phosphate buffer instead of Tris HCl buffer. A 3 mL solution containing appropriate concentration of BSA (5 µM) was titrated by successive additions of 5 µL stock solution of compounds (0-40 µM). Simultaneously, synchronous fluorescence spectra of the mixture were recorded in the range of 270-400 nm by setting $\Delta\lambda$ =15 nm and $\Delta\lambda$ =60 nm (difference between the excitation and emission wavelengths of BSA) for tyrosine and tryptophan residues respectively. UV absorption spectra of BSA were recorded in phosphate buffer in the absence and presence of increasing concentration of compounds.

2.5. Antioxidant assays

In vitro radical scavenging assays were performed in triplicate and standard deviation of absorbance was less than 10% of the mean. Ascorbic acid (AA) and butylated hydroxyl anisole (BHA) are used as positive control in all assays. 1,1-diphenyl-2-picrylhydrazyl (DPPH) free radical scavenging activity was measured using the method described by Shih-Chuan Liu et al [24]. Total antioxidant activity assay was studied using ABTS radical cation decolourisation assay [25]. The effect of super oxide radical scavenging activity was determined by the nitroblue tetrazolium reduction method and described by Wei Fu et al [26]. Nitric oxide (NO) scavenging activity was performed based on the Griess assay [27]. For the above four assays, all of the tests were run in triplicate and the percentage of activity was calculated using the formula:

$$\%\ \text{of scavenging capacity} = \frac{A_0 - A_c}{A_0} \times 100 \quad (1)$$

A_0 and A_c are the absorbance in the absence and presence of the tested compounds, respectively. The 50 % activity (IC_{50}) can be calculated using the percentage of activity.

2.6. Antimicrobial assay

The antibacterial activity of the prepared ligand and its silver complex were tested *in vitro* against three gram-positive bacteria *Bacillus subtilis, Staphylococcus aureus*, and *Stapylococcus albush* and three gram-negative bacteria *Salmonella paratyphi, Escherichia coli* and *Klebsella pneumonia* using agar-well diffusion method [28, 29]. Antifungal activities of the compounds were screened against *C.albicans, A.fumigates* and *A.niger* using disc diffusion method. Also, the minimum concentrations of the synthesised compounds to inhibit the microorganisms (MIC) were determined by the micro broth dilutions technique strictly following the National Committee for Clinical Laboratory Standards (NCCLS) recommendations [30, 31]. In all determinations, tests were performed in duplicate and the results were reported as mean of these values.

2.7. Evaluation of cytotoxicity

The inhibitory concentration (IC_{50}) value was evaluated using an MTT [3-(4,5-dimethylthiazol-2-yl)-2,5-diphenyltetrazolium bromide] assay. The optical density was measured at 620 nm in an ELISA multiwell plate reader (Thermo Multiskan EX, USA). The OD value was used to calculate the percentage of viability using the following formula.

$$\%\ \text{of viability} = \frac{\text{OD value of experimental sample}}{\text{OD value of experimental control}} \times 100 \qquad (2)$$

2.7.1. Morphological study & Fluorescence microscopic analysis

The MCF-7cells that were grown on cover slips (1×10^5 cells/cover slip) incubated for 6-24 h with compounds at the IC_{50} concentration and the mono layers per experimental group were photo micrographed. Approximately 1µL of a dye mixture (100 mg/mL acridine orange (AO) and 100 mg/mL ethidium bromide (EtBr) in distilled water) was mixed with 9 mL of cell suspension (1×10^5 cells/mL) on clean microscope cover slips. The selected cancer cells

were collected, washed and stained with 1 mL of AO/EtBr. After incubation for 2 min, the cells were visualized with an excitation filter at 480 nm. Likewise the cells were placed on glass coverslip in a 24-well plate and treated with complex for 24 h. The fixed cells were permeabilised with 0.2% triton X-100 (50 μL) for 10 min at room temperature and incubated for 3 min with 10 μL of DAPI by placing a coverslip over the cells to enable uniform spreading of the stain.

3. Results and discussion

The ligand (**H_2L**) was prepared by the condensation reaction of α-keto glutaric acid with methyl carbazate (**Scheme 1**). Silver complex was isolated by stoichiometric (1:2) reaction of silver nitrate with the ligand. Repeated crystallisation of the mother liquor yielded crystalline silver complex. Both the ligand and complex were soluble in water, alcohol and DMSO. They were characterised by elemental analysis, FT-IR, UV-Vis, NMR (^{1}H & ^{13}C) and TG-DTA measurements. Further, the formation of both the ligand and complex were characterised by single crystal X- ray diffraction.

3.1. Spectroscopic Characterisation

The IR spectra provide valuable information regarding the nature of functional groups present in both ligand and complex (**Fig. S1**). Solid state FT-IR spectrum of the ligand shows sharp doublet at 3607, 3476 cm^{-1} assigned to O-H vibrations of lattice water and carboxylic group respectively. The ν(C=N) stretching vibration is found at a lower frequency for silver complex (1585 cm^{-1}) than the ligand (1602 cm^{-1}) indicating the involvement of azomethine nitrogen towards metal coordination. The asymmetric and symmetric stretching frequencies of the coordinated carboxylate group are seen in 1545, 1360 cm^{-1}, respectively with a separation $\Delta\nu$ ($\nu_{asym} - \nu_{sym}$) of 185 cm^{-1} indicating monodentate coordination of carboxylate ion [32]. The electronic spectra of the ligand and complex were recorded in aqueous medium. The broad band observed at 240 and 290 nm could be assigned to n–π* and π–π* transitions

respectively within the organic ligand. Minor shift with increase in intensity was observed for the complex, which may be attributed to the chelation of ligand.

The ^{1}H and ^{13}C NMR spectra (**Fig. S2-S5**) have been recorded for the ligand and complex in DMSO-d6 solution and the peak assignments are compared with the literature values [17, 33]. In ^{1}H NMR spectrum of the ligand, appearance of an important signal at 10.73 ppm has been assigned to NH proton; in complex this signal is shifted to 8.30 ppm. A peak at 3.73 ppm is due to $–OCH_3$ proton, where as in complex two signals appearing at 3.74 and 3.65 ppm indicate that the two methoxy protons are magnetically nonequivalent and are in different chemical environment around metal. A peak at 3.71 ppm with an integration corresponds to two protons is assigned for a water molecule in the ligand. The methylene protons of ligand nearer to carboxylic and azomethine groups are observed in the region between 2.69-2.65 and 2.38-2.34 ppm respectively [33]. In complex, methylene protons are observed as four triplets in the range of 2.73-2.35 ppm corresponding to two independent (neutral and anionic) ligands.

In the ^{13}C NMR spectra of ligand and complex, the carboxylic carbon (-COOH) signals appear in the most downfield region at 173 and 165 ppm for C7 & C1 carbons respectively. For the ligand, signals of carbonyl (C3) and azomethine (C2) carbons are noticed at 154 and 143 ppm respectively. In the complex, these signals exhibited largest upfield shift to 79 ppm due to the closest proximity of these atoms to the central metal ion [34]. In both the ligand and complex, the methoxy (C4) carbons gave signal at 52 ppm and methylene carbons appear at 29 and 21 ppm for C6 & C5 respectively.

3.2. Stability in aqueous media

Rapid (AgCl) precipitation in biological media results severe problem in treatment of silver based drugs with wounds. Effective treatment of infections requires sustained release

of silver ions to the infections which were focused by researchers [35]. In this context, water soluble silver complex was subjected by stability measurements in water at 37 °C. As shown in **Fig. S6**, silver complex slowly releases Ag^+ ions and confirm its silver donating ability to the targets. Periodic assessment of absorption spectrum over a period of 90 min reveals that the transitions in spectrum slowly transfers to the spectrum of free ligand [36], after that there is no change in absorption spectrum.

3.3. Thermal analysis

In order to further characterize these compounds in terms of thermal stability, their thermal behaviour was investigated by simultaneous TG-DTA under air that is shown in **Fig. S7**. A summary of thermal data of the compounds are presented in **Table S1** with the decomposition of intermediates and final products best fitted with the corresponding mass loss in TG curve. Simultaneous TG-DTA of the ligand shows an endothermic decomposition at 150 °C to give ethanimine as an intermediate with the mass loss of 82.50% (Calcd. 81.36%). This kind of carbazate Schiff bases are known to decompose via ethanimine intermediate [12]. Then the intermediate decomposes exothermically with almost 100% mass loss to give gaseous products.

The network of silver complex was stable up to 200 °C, above that the framework start to collapse. An abrupt mass loss at 218 °C accompanied by the endothermic decomposition of organic components leads to the formation of silver propionate as a probable intermediate (Obsd. 67.00%, Calcd. 66.73%). The decomposition ended at 600 °C in which, the DTA curve shows a strong exothermic peak (500 °C) due to the loss of the carboxylate ligand and formation of metallic silver as the final decomposition product (Obsd. 19.5%, Calcd. 19.9%). It has been observed that thermal degradation of silver complex led to the formation of metallic silver [37]. Powder X-ray diffraction studies were performed to determine the crystalline nature and phase purities of complex and the silver. **Fig S8** shows the X-ray

diffractograms of complex and silver. The PXRD patterns exhibit number of peaks that are sharp and intense indicating their pure and highly crystalline nature. Four distinct diffraction peaks are observed at 2θ values of 38.2°, 44.3°, 64.5° and 77.4°, corresponding to the (111), (200), (220) and (311) reflections of cubic Ag (JCPDS No. 4-0783). The surface morphological feature of metallic silver was studied by FESEM. Detailed FESEM micrographs are presented in **Fig. S9** with magnification of 15,000 was shown to be sheet like pattern. EDX elemental analysis indicates that the sheet composed of pure silver. The observation of larger nano particles may be attributed to the fact that they have a tendency to agglomerate due to the high surface energy of ultrafine nanoparticles.

3.4. Crystal Structure

X-ray crystallography reveals that both the ligand and complex crystallize in monoclinic crystal system with the space group of $P2_1/c$ (**Figs. 1a** & **1b**). Crystal data and details of structure refinement are given in **Table 1**. Selected bond lengths and bond angles are listed in **Table S2**. Hydrogen bonding parameters are given in **Tables S3 & S4.**

The ligand possesses condensed unit of ketoglutaric acid and methyl carbazate with a lattice water molecule as asymmetric unit with Z=4. The schiff base formation was verified by comparing the bond distances. The C2-N1 bond distance is 1.28(4) Å that is appreciably close to that of C=N double bond, confirming the formation of Schiff base ligand [38]. The bond distance of C3-O3 is 1.218(4) Å which is very close to C=O bond length (1.21 Å). Schiff base ligands are linked through oxygen atom of water molecule (O1W) and forming hydrogen bonds (strong O-H...O, N-H...O and weak C-H...O interactions) to generate 1D chain parellel to *a* axis (**Fig S10)**. In addition to that one of the carbonyl oxygens (O1) of carboxyl group forms bifurcated acceptor from O-H and C-H group of adjacent ligand. Surprisingly, the solvated water molecule acts as a linker between the chains and generate $R_2^2(8)$ ring motif. And also noticed that the carbonyl group of carbazate moiety acts as bifurcated acceptor from the lattice water molecles.

In [Ag(H_2L)(HL)], silver atom is hexa-coordinated with distorted octahedral environment being bonded to two tridentate hydrazone ligands. In the complex, both the neutral and uni-negative ligands are coordinated to the metal in a tridentate N,O,O chelate fashion. The two carboxylate entities of the ligand in the complex are not equivalent; O2A is protonated, while O2B is not, and resulting overall complex as neutral. This assessment is entirely supported by the fact that much shorter Ag to O1B (charged) distance of 2.475Å compared to 2.505Å for the protonated carboxylic acid (**Fig. S11**). Two Schiff base ligands found to be coordinated via azomethine nitrogen, carbonyl oxygen of methyl carbazate and carboxylic oxygen of acid resulting four five membered chelate rings around the metal with bite angles of 66.09, 66.80, 66.16 and 67.00˚. The angle between the plans passing through the ligands is 83.66˚, indicating that the neutral and negatively charged ligands are nearly perpendicular to each other. The crystal packing of complex is largely achieved through O-H...O, N-H...O and C-H...O hydrogen bonds. The oxygen (O5) atom from uncoordinated acid group plays a bifurcated acceptor from the O6 of adjacent ligand generating 1D wave like chain. Two adjacent antiparallel chains are connected by C-H...O5 hydrogen bonding from the methyl group of carbazate. In addition to that, interestingly, O2A atom acts as bifurcated donor to the oxygen atoms (O1B, O2B) of coordinated carboxylic group of adjacent chain creating 2D network (**Fig. S12**). As a whole, anhydrous neutral silver complex creates extended structure by means of various hydrogen bonds to generate 3D supramolecular network.

3.5. DNA binding studies

Biochemical evaluation of silver(I) complexes is related mostly to their action, which appears to involve interaction with DNA. Moreover, DNA is the major target of many anticancer drugs. Electronic absorption spectra were carried out to examine the bonding mode and ability with CT-DNA [39]. The interaction of ligand and complex with CT-DNA

was followed by recording the UV- Visible spectra in fixed concentrations (**Fig S13**). Upon addition of CT-DNA, an increase in absorption intensity in the range of 210-300 nm, a hyperchromism of ligand centred transition was observed. These observations indicate that there are non- classical external intercalation between CT-DNA and compounds which might be electrostatic and/or groove binding modes or the compounds could uncoil the helical structure of DNA. These indicate that the compounds possess strong affinity towards DNA. Furthermore, the binding mode is proved through displacement studies

3.5.1. Competitive studies with ethidium bromide

Ethidium bromide (EB-3,8- diamino-5-ethyl-6-phenyl-phenanthridium bromide) is a standard intercalator forming stable complex with CT-DNA and emits intense fluorescence due to the interaction of planar phenanthridium ring between adjacent base pair in the double helix. The emission of spectra of EB-DNA system in the absence and presence of ligand and complex are shown in **Fig S14**. Reduction in fluorescence intensity of DNA-EB system by about 18.41 and 33.86 % observed for ligand and silver complex respectively. These results indicate that the compound would effectively compete with EB for binding sites on DNA [40, 41]. The relative quenching efficiency of the compounds to CT-DNA was determined by the classical Stern-Volmer equation [42, 43]

$$\frac{F^0}{F} = 1 + K_{sv}[Q] \quad (3)$$

Here F^o and F are the fluorescence intensities in the absence and the presence of the quencher, respectively. K_{SV} is the Stern–Volmer dynamic quenching constant and $[Q]$ is the total concentration of the quencher. The linear fit plot of F^0/F versus [complex]/ [DNA], K_{SV} is given by the ratio of the slope to intercept. The K_{SV} value of ligand and complex were calculated as 2.47×10^5 and 4.75×10^5 M^{-1} respectively. The slightly higher binding constant of complex implies that it relatively has better interaction with DNA as compared to ligand.

3.6. Albumin binding studies

Bovine serum albumin (BSA) is the most abundant transport protein in blood plasma and the interaction between antitumor drugs and BSA may have effect on their bioavailability and toxicity [44-46]. It is of great interest to use quenching of the intrinsic tryptophan fluorescence of BSA (Trp-212 and Trp-134) as a tool to study the interaction of BSA with the synthesised compounds [47, 48]. Fluorescence titration studies have been performed using 5 μM BSA and varying the concentration of compounds (0–40 μM) in the range 290–500 nm. The effect of compounds upon addition on the fluorescence emission spectra of BSA is shown in **Fig S15**. The fluorescence intensity of BSA at ~348 nm quenched with no shift up to 28.8% and 35.7% of the initial intensity of BSA for the ligand and Ag (I) complex, respectively. The type of quenching progression was explored by the absorption spectra of BSA. Dynamic quenching affects only the excited state of fluorophore (not changing the absorption spectrum), whereas static quenching leads to perturbation of fluorophore. The emission intensity of BSA increases as the addition of compounds with small blue shift, revealing the existence of static quenching [49].

To investigate the structural changes that occurred in BSA upon the addition of compounds, synchronous fluorescence spectra of BSA were measured [50]. According to Miller, in synchronous fluorescence spectroscopy the difference between the excitation and emission wavelengths ($\Delta\lambda = \lambda em - \lambda ex$) reflects the spectra of a different nature of chromophores [51]. If the $\Delta\lambda$ value is 15 nm, the synchronous fluorescence of BSA is characteristic for tyrosine residue, whereas $\Delta\lambda$ value of 60 nm is characteristic for tryptophan residue [52]. The effect of compounds on synchronous fluorescence spectra of BSA are shown in **Figs. S16** & **S17** of ESI. It is apparent that the intensity of Trp or Tyr residues decreases in the presence of ligand and complex. Tyr emission intensity was found to decrease up to 14.5 and 25% whereas Trp fluorescence emission showed significant decrease

of about 23.3 and 30.6% for ligand and silver complex respectively. However, the emission peak position of Trp or Tyr residues does not show significant shift, indicating that the polarity around Trp or Tyr residues is unchangeable [53]. So, the presence of compounds does not obviously affect the ??-helical conformation of BSA.

3.6.1. Binding Parameters

Florescence quenching data were analysed to obtain various binding parameters and quenching progression for the interaction of compounds and BSA. The quenching data were analysed with Stern-Volmer and Scatchard equation [54]. The quenching constant (Kq) was calculated using the plot of $??_0/??$ versus [??] giving a straight line, and Kq is thus obtained from the slope of the diagram (**Fig 2**). The values of Kq obtained are 4.1×10^5 & 5.4×10^6 M^{-1} at 298 K for ligand and complex respectively. Static quenching binding constant (K) and number of binding sites can be determined using the following Scatchard eqn (4)

$$log\left[\frac{F_O - F}{F}\right] = logK + nlog[Q] \quad (4)$$

Where K is the binding constant of quencher, determined from the slope of *log [(F₀ − F)/F]* versus *log [Q]* as shown in inset plot **Fig. S15**. The calculated value of binding constant (K) for ligand and its complex with BSA was found to be 9.05×10^5 and 1.15×10^6 M^{-1} and the number of binding sites (n) was 0.73 and 0.87 respectively. Little higher magnitude of Kq & K for Ag complex compared to that of free ligand indicated a higher affinity of metal towards protein environment.

3.7. Antioxidant assays

To investigate the antioxidant activity of both the ligand and its silver complex *in vitro*, $ABTS^{\bullet+}$, $DPPH^{\bullet}$, $NO^{\bullet}$, $O_2^{\bullet-}$ scavenging assays were carried out based on the decay of free radical UV-Vis absorbance quenched by antioxidants [55]. The IC_{50} values for compounds and standard (natural Ascorbic acid (AA) and synthetic Butylated hydroxyl anisole (BHA)) antioxidants against free radicals are displayed in **Fig. 3**.

Free radicals are known to be a major factor in biological damages, and $DPPH^{\bullet}$ has been used to evaluate the free radical scavenging activity of natural antioxidants [56, 57]. The antioxidant present in sample reacts with DPPH radical and converts into reduced form either by donating hydrogen atom or transferring electron followed by proton [58]. From the results, both the ligand and complex with an IC_{50} value of 9.31 and 12.48 mg/mL respectively indicate that they have the ability to scavenge free radicals and could serve as a strong free radical inhibitor or scavenger according to standard. ABTS assay is an excellent tool for determining the antioxidant activity of hydrogen-donating antioxidants and of chain-breaking antioxidants [59]. The compounds efficiently scavenged ABTS radicals generated by the reaction between ABTS and potassium persulfate. The ligand exhibited an IC_{50} value of 16.58 mg/mL somewhat comparable with silver complex (34.49 mg/mL). Superoxide radical, known to be very harmful to cellular components as a precursor of the more reactive oxygen species, contributes to tissue damage and various diseases [60]. The superoxide anion radicals $O_2^{\cdot -}$ scavenging activity was determined by nitro blue tetrazolium (NBT) method. Scavengers present in the sample compete with NBT for radicals and slowdown the formation of blue colour, which is quantitatively measured at 560nm [61]. $[Ag(HL)(H_2L)]$ shows an excellent superoxide radical scavenging activity comparable to both standards with the IC_{50} value of 9.46 mg/mL. Sodium nitroprusside in aqueous solution at physiological pH spontaneously generates nitric oxide, interacts with oxygen to produce nitrite ions, which can be estimated by Griess reagent [62]. The activity of ascorbic acid (36.12 mg/mL) is comparable with those of ligand (35.88 mg/mL) than that of other fractions. It has been reported that the antioxidant activity of compounds may result from the neutralization of free radicals initiating oxidation processes, or from the termination of radical chain reactions, due to their hydrogen donating ability [57].

3.8. Anti microbial activity

The *in vitro* biological activity has been evaluated qualitatively for its anti-microbial and anti-fungal activities (average of three determinations) using disc diffusion method against three gram positive bacteria *Bacillus subtilis, Staphylococcus aureus,* and *Stapylococcus albush* and three gram negative bacteria *Salmonella paratyphi, Escherichia coli* and *Klebsella pneumonia* along with fungi *C.albicans, A.fumigates* and *A.niger* at concentration 100 µg/mL. *Ciprofloxacin* (10 µg/mL) was used as positive control, while DMSO as the solvent to prepare the stock solution play no role in growth inhibition of the bacteria [63]. Antimicrobial activity of silver has been known for a long time and is attributable to the silver cation Ag^{+}, which binds strongly to electron donor groups (sulfur, oxygen and nitrogen) present in biological molecules. Screening data of anti microbial activities are given in **Table 2**. From the zone of inhibition diameter data, it's clear that the metallic silver and complex show great activity against both of the gram negative and gram positive bacteria, while there is little moderate inhibition zone observed for ligand. The activity of ligand might be due to the presence of azomethine group that play an important role. In particular, complex shows excellent activity against the *Escherichia coli* (G^{-}) and *Staphylococcus aureus* (G^{+}) bacterium comparatively lower than the drug reference. This difference in the activity of ligand and corresponding Ag(I) complex was explained by Tweedy's chelation theory [64]. The activity might be due to the liphophilic nature of complex upon chelation of metal, which in turn resulted by the increase in electron delocalisation. However, they exhibited obviously enhanced activity against fungus C. albicans. Minimum inhibitory concentrations (MICs) were determined as a representative against *Escherichia coli* (G^{-}) *Staphylococcus aureus* (G^{+}) and *C.albicans* by the broth micro dilution method. Silver and its complex show remarkable activity against *Escherichia coli* with the MIC value of 40.2 and 31.3 µg/mL respectively. However, moderate activity is found for *Staphylococcus aureus and* yeast (*C.albicans*).

3.9. Cytotoxicity assay

Since ligand and complex have the ability to bind DNA and BSA, in order to evaluate the antitumor activity of complex in comparison to free ligand, we examined the effect of synthesized ligand and silver complex on the cell response of the human breast cancer (MCF-7) cell line by using the MTT assay and compared to reference Doxorubicin (DOX). Silver in various forms (nanoparticles, coordination complexes and organometallic compounds) is now being focussed due to its significant effect against cancer cells [65]. **Fig. S18** shows the *In vitro* cytotoxic activity of compounds (10-100 μM concentrations) against selected cancer cells. The IC_{50} values of compounds against 27±1.5 (**H_2L**), 24±1.3 μM [**Ag(HL)(H_2L)**] inhibitory concentration obtained for MCF-7 breast cancer cells. In the same condition, the IC_{50} of DOX was found to be 18±0.9 μM. Compared to ligand, silver complex has shown better cytotoxicity. This could be attributed to the presence of silver ion that synergistically increased the cytotoxicity. Most important criteria for an anti cancer drug is to show minimum or no side effects to the normal cells in addition to the tumour cells of the patients. In addition, the cytotoxic activities of the compounds were also evaluated against normal human breast cells HBL-100 (**Fig. S18**). From the result it was observed that both the ligand and complex were non toxic to normal cell.

3.9.1. Cell morphoslogy & Fluorescence microscopy analysis

Morphological changes induced in MCF-7 human breast cancer cells after treatment of compounds with their respective inhibitory concentration for 24 h are shown in **Fig. 4**. Phase-contrast micrographs reveal that the compound induces increased cell shrinkage, membrane blebbing and forms floating cells, compared to the control in a dose-dependent manner (**Fig. 4 b-d**).

To elucidate the apoptotic activity of synthesized compounds, apoptotic staining fluorescence microscopic analysis was carried out. Acridine orange- Ethidium bromide (AO-

EtBr) staining uses a combination of two dyes to visualise cells with aberrant chromatin organisation [66]. Fluorescence microscopy images of MCF-7 cancer cells in the absence (Control) and presence of compounds are shown in **Fig. 5.** The control viable cells have uniformly green fluorescing nuclei. After treatment of cells with compounds, we have observed morphological changes such as presence of late apoptotic cells that have orange to red nuclei with condensed or fragmented chromatin and necrotic cells. The results indicate that the silver complex induce cell death through apoptosis compared to that of ligand.

In order to further confirm the nuclear condensation and fragmentation of compounds on selected cancer cells we evaluated the DAPI staining method. 4,6-diamidino-2-phenylindole-2-HCl (DAPI) binds DNA providing a blue fluorescence when viewed under ultraviolet light. Fluorescence microscopy images of breast cancer cells after 24 h stained with DAPI in the presence and absence of compounds are shown in **Fig. 6.** It is found that compounds (**Fig. 6 b-d)** shown higher level of nuclear fragmentation and the untreated cells do not show any significant changes in the nuclear appearance**.** Complex treated MCF-7 cancer cells shows bright fetches which indicate the condensed chromatins and nuclear fragmentations in the cancer cells and is comparable to the control and found to be significant.

4. Conclusion

In conclusion, new 2**-(Methoxycarbonyl-hydrazono)-pentanedioic acid** and its silver complex have been synthesised and characterised by elemental, spectral and thermal analyses. Single crystal XRD analysis strengthens the evidence of physicochemical characterisation. The groove binding mode of CT-DNA and static binding mode of BSA towards complex was identified by UV-Visible absorption and emission measurements. The complex was effective towards bacteria and fungi cells, in particular to *Escherichia coli* (G^-) and *Staphylococcus aureus* (G^+) bacterium. Cytotoxicity reveals that the complex acts as a

potential anticancer agent by inducing phenotypical changes, like increasing the membrane permeability, nuclear fragmentation and finally apoptotic cell death. It appears that the silver complex is more likely to become antibiotics [67] than anticancer drugs [68]. These findings give a clear indication that the complex has the potential to serve as a biomaterial in various aspects of chemotherapeutic agents. The synthesis of metal complexes using Schiff bases derived from methyl and ethyl carbazate analogues as ligands is in progress and will be reported in due course.

Acknowledgement-

S.P gratefully acknowledges the financial assistance received from the Women Scientist Scheme – WOS (A), Department of Science and Technology, New Delhi, India [Grant No. SR/WOS(A)/CS-42/2013]. S.G is thankful to University Grants Commission, New Delhi for the award of UGC-Emeritus Fellowship.

Appendix A. Supplementary data

The following is the supplementary data related to this article:

CCDC 1545009 and 1546023 contain the supplementary crystallographic data for **H_2L** and **[Ag(HL)(H_2L)]**, respectively. These data can be obtained free of charge *via* http://www.ccdc.cam.ac.uk/conts/retrieving.html, or from the Cambridge Crystallographic Data Centre, 12 Union Road, Cambridge CB2 1EZ, UK; fax: (+44) 1223-336-033; or E-mail: deposit@ccdc.cam.ac.uk.

References

[1] T. L. Zhang, J. C. Song, J. G. Zhang, G. X. Ma, K. B. Yu, Z. Naturforsch 60b (2005) 505-510.

[2] G. Ma, T. Zhang, K. Yu, J. Braz. Chem. Soc. 16 (2005) 796-800.

[3] K. Srinivasan, S. Govindarajan, W.T.A. Harrison, J. Coord. Chem. 64 (2011) 3541-3550.

[4] A. Kathiresan, K. Srinivasan, S. Brinda, M. Nethaji, S. Govindarajan, Transit. Met. Chem. 37 (2012) 393-397.

[5] K. Srinivasan, A. Kathiresan, S. Govindarajan, J. T. Aughey, W. T. A. Harrison, J. Coord. Chem. 67 (2014) 857-869.

[6] K. Srinivasan, A. Kathiresan, W. T. A. Harrison, S. Govindarajan, J. Coord. Chem.

67 (2014) 3324-3334.

[7] C. Sitong, G. Weiming, Z. Bo, Z. Tonglai, Y. Li, Polyhedron 117 (2016) 110-116.

[8] S. T. Chen, W. M. Guo, T. L. Zhang, J. Coord. Chem. 69 (2016) 2610-2619.

[9] R. Bergs, K. Sunkel, Christoph Robl, W. Beck, J. Organomet. Chem. 533 (1997) 247-255.

[10] P. Nithya, J. Simpson, S. Govindarajan, Polyhedron 141 (2018) 5–16.

[11] P. Nithya, S. Helena, J. Simpson, M. Ilanchelian, A. Muthusankar, S. Govindarajan, J. Photochem & Photobiol. B165 (2016) 220–231.

[12] P. Nithya, J. Simpson, S. Helena, R Rajamanikandan, S. Govindarajan, J. Therm. Anal. Calorim. 129 (2017) 1001–1019.

[13] P. Nithya, J. Simpson, S. Govindarajan, Inorg. Chim. Acta 467 (2017) 180–193.

[14] Z. Shokohi pour, H. Chiniforoshan, A.A. Momtazi borojeni, B. Notash, J. Photochem. Photobiol. B62 (2016) 34–44.

[15] J. Lu, Q. Sun, J.-L. Li, L. Jiang, W. Gu, X. Liu, J.-L. Tian, S. P. Yan, J. Inorg. Biochem. 137 (2014) 46–56.

[16] W. Bal, M. Sokolowska, E. Kurowska, P. Faller, Biochim. Biophys. Acta 1830 (2013) 5444–5455.

[17] M. Belicchi Ferrari, F. Bisceglie, G. Gasparri Fava, G. Pelosi, P. Tarasconi, R. Albertini, S. Pinelli, J. Inorg. Biochem. 89 (2002) 36–44.

[18] M. Baldini, M. B. Ferrari, F. Bisceglie, P. P. Dall Aglio, G. Pelosi, S. Pinelli, P. Tarasconi, Inorg. Chem. 43 (2004) 7170-7179.

[19] J. Marmui, J. Mol. Biol. 3 (1961) 208-218.

[20] CrysAlisPro Software System, Agilent Technologies UK Ltd, Yarnton, Oxford, UK (2015).

[21] L. J. Bourhis, O. V. Dolomanov, R. J. Gildea, J. A. K. Howard and H Puschmann, Acta Crystallogr. A71 (2015) 59-71.

[22] O.V. Dolomanov, L. J. Bourhis, R. J. Gildea, J. A. K. Howard and H. Puschmann, J. Appl. Cryst. 42 (2009) 339-341.

[23] G.M. Sheldrick, A short history of ShelX, Acta Crystallogr. A64 (2008) 339-341.

[24] C.L. Shih, T. L. Jau, K. W. Chin, Y. C. Hsin, J. Y. Deng, Food Chem. 114 (2010) 577-581.

[25] R. Re, N. Pellegrini, A. Proteggente, A. Pannala, M. Yang and C. Rice Evans, Free Radical Biol. Med. 26 (1999) 1231–1237.

[26] F. Wei, C. Jinglou, C. Yaling, L. Yongfang, C. Liming, P. Lei, J.

Ethnopharmacol. 130 (2010) 521-528.

[27] L. C. Green, D. A. Wagner, J. Glogowski, P. L. Skipper, J. S. Wishnok and S. R. Tannenbaum, Anal. Biochem. 126 (1982) 131–138.

[28] R. M. Maurya, M. N. Jayaswal., V. G. Puranik, P. Chakrabarti, S. Gopinathn, C. Gopinathan, Polyhedron 16 (1997) 3977-3983.

[29] S. Irshad, M. Mahmood, F. Perveen, Res. J. Biol. 2 (2012) 1–8.

[30] CLSI, Approved Standard, M07–A9, Wayne, PA, USA, 2012.

[31] A. Cinarli, D. Gürbüz, A. Tavman, A.S. Birteksöz, Chin. J. Chem. 30 (2012) 449–459.

[32] K. Nakamoto, Infrared and Raman Spectra of Inorganic and Coordination Compounds (Part B), John Wiley and Sons, New York, 6th edn, 58 (2009) 65.

[33] M. Baldini, M. Belicchi Ferrari, F. Bisceglie, S. Capacchi, G. Pelosi, P. Tarasconi, J. Inorg. Biochem. 99 (2005) 1504–1513.

[34] M. Milenkovic , A. Bacchi, G. Cantoni, J. Vilipic , D. Sladic, M. Vujcic , N. Gligorijevic, K. Jovanovic, S. Radulovic, K. AnCelkovic, Eur. J. Med. Chem. 68 (2013) 111-120.

[35] (a) T.R. deBoer, I. Chakraborty, M.M. Olmstead, P.K. Mascharak, Cryst. Growth Des. 14 (2014) 4901–4905; (b) S.W. Jaros, P. Smolenski, M.F.C. Guedes da Silva, M. Florek, J. Krol, Z. Staroniewicz, A.J.L. Pombeiro, A.M. Kirillov, Cryst Eng Comm. 15 (2013) 8060–8064.

[36] J. Jimenez, I. Chakraborty, M. Rojas Andrade, P. K. Mascharak, J. Inorg. Biochem. 168 (2017) 13–17.

[37] N. E. A. El- Gamel, Dalton Trans. 42 (2013) 9884-9892.

[38] A. S. Girgis, J. Chem. Res. 2 (2006) 81-83.

[39] E. C. Long and J. K. Barton, Acc. Chem. Res. 23 (1990) 271-273.

[40] J. B. Lepecq and C. Paoletti, J. Mol. Biol. 27 (1967) 87-106.

[41] M. Lee, A. L. Rhodes, M. D. Wyatt, S. Forrow, J. A. Hartley, Biochemistry 32 (1993) 4237-4245.

[42] J. R. Lakowicz and G. Weber, Biochemistry 12 (1973) 4161-4170.

[43] K. S. Ghosh, B. K. Sahoo, D. Jana and S. Dasgupta, J. Inorg. Biochem. 102 (2008) 1711-1718.

[44] L. Trynda-Lemiesz and M. Łuczkowski, Journal of Inorg Biochem 98 (2004) 1851-1856.

[45] L. L. Yan, X. Y. Wang, Y. Q. Wang, Y. M. Zhang, Z. J. Guo, J. Inorg.

Biochem. 106 (2012) 46–51.

[46] P. B. Kandagal, S. Ashoka, J. Seetharamappa, S. M. T. Shaikh, Y. Jadegoud, and O. B. Ijare, J. Pharm. & Biomed. Anal. 41 (2006) 393–399.

[47] V. Anbazhagan and R. Renganathan, J. Luminescence 128 (2008) 1454–1458.

[48] J. Liu, J. Tian, Y. Li, X. Yao, Z. Hu, and X. Chen, Macromol. Biosci. 4 (2004) 520–525.

[49] (a) J. R. Lakowicz, Fluorescence Quenching: Theory and Applications. Principles of Fluorescence Spectroscopy, Kluwer Academic/Plenum Publishers, New York, 1999 53127; (b) X. Z. Feng, Z. Yang, L. J. Wang, C. Bai, Talanta 47 (1998) 1223-1229.

[50] G. Z. Chen, X. Z. Huang, Z. Z. Zheng, J. G. Xu, Z. B. Wang, Methods of Fluorescence Analysis, 2nd edn, Science Press, Beijing, 1990.

[51] J. N. Miller, Proc.: Anal. Div. Chem. Soc., 16 (1979) 203–208.

[52] J. H. Tang, F. Luan, X. G. Chen, Bioorg. Med. Chem., 14 (2006) 3210–3217.

[53] X. F. Liu, Y. M. Xia, Y. Fang, J. Inorg. Biochem. 99 (2005) 1449–1457.

[54] (a) J. R. Lakowicz, Principles of Fluorescence Spectroscopy, Kluwer Academic/Plenum Publishers, New York, 3rd edn, 2006. (b) B. Manimaran, L.J. Lai, P. Thanasekaran, J.Y. Wu, R.T. Liao, T.W. Tseng, Y.H. Liu, G.H. Lee, S.M. Peng and K. L. Lu, Inorg. Chem. 45 (2006) 8070–8077.

[55] Z. Q. Liu, Chem. Rev. 110 (2010) 5675–5691.

[56] T. Yokozawa, C.P. Chen, E. Dong, T. Tanaka, G.I. Nonaka, I. Nishioka, Biochem. Pharmacol. 56 (1998) 213-222.

[57] Y. Chung, S. Chen, C. Hsu, C. Chang, S. Chou, Food Chem. 91 (2005) 419-423

[58] N. Etsuo, Free Radic. Biol. Med. 49 (2010) 503-515.

[59] L. P. Leong, G. Shui, Food Chem. 76 (2002) 69-75.

[60] S. Sakanaka, Y. Tachibana, Y. Okada, Food Chem. 89 (2005) 569-574.

[61] P. Irene, V. Francesc, B. Jaume, R. R. Alfredo, S. Gloria, M. M. Antonia, Life Sciences 73 (2003) 1667-1681.

[62] L. C. Green, D. A. Wagner, J. Glogowski, P. L Skipper, J. S Wishnok, S. R. Tannenbaum, Anal Biochem. 126 (1982) 131-138.

[63] W. Streciwilk, J. Cassidy, F. Hackenberg, H. Müller-Bunz, F. Paradisi, M. Tacke, J. Organomet. Chem. 749 (2014) 88-99.

[64] B. Tweedy, Phytopathology 55 (1964) 910-914.

[65] (a) H. A. Mohamed, B.R. Lake, T. Laing, R.M. Phillips, C.E. Willans, Dalton Trans. 44 (2015) 7563-7569; (b) R.A. Haque, S.Y. Choo, S. Budagumpi, M.A. Iqbal, A.A. A. Abdullah, Eur. J. Med. Chem. 90 (2015) 82-92.

[66] J. Steigerova, J. Oklestkova, M. Levkova, L. Rarova, Z. Kolar, M. Strnad, Chem. Biol. Interact. 188 (2010) 487-496.

[67] N. Browne, F. Hackenberg, W. Streciwilk, M. Tacke, K. Kavanagh, Biometals 27 (2014) 745 - 752.

[68] I. Fichtner, D. Behrens, J. Cinatl jr., M. Michaelis, L. C. Sanders, R. Hilger, B. N. Kennedy, A. L. Reynolds, F. Hackenberg, G. Lally, S. J. Quinn, I. McRae, M. Tacke, Letters in Drug Design & Discovery 9 (2012) 815 – 822.

Scheme 1 Synthesis of Ligand (**H_2L**) and complex **[Ag(HL)(H_2L)]**

Fig. 1. X-ray molecular structure of **$H_2L.H_2O$ (a)** and **[Ag(HL)(H_2L)] (b)** with atom labelling scheme (thermal ellipsoids are plotted at 50% probability).

Fig. 2 Plot of F^0/F vs. [Q]

Fig. 3 Trends in inhibition of various radicals by ligand and complex along with the standard AA and BHA.

Fig. 4 Microscopic images of MCF-7 cancer cells treated with compounds (ctrl (a), 10(b), 20(c), 40μM (d))

Fig. 5 AO/EtBr staining of MCF-7 cells using fluorescence microscopy after treatment with ligand and complex (0(a), 10(b), 20(c), 40 μM(d)) for 24 h.

Fig. 6 Fluorescence microscopic images of MCF-7 cells after treatment with ligand and complex (0(a), 10(b), 20(c), 40μM (d)) for 24 h. Cells were stained with DAPI

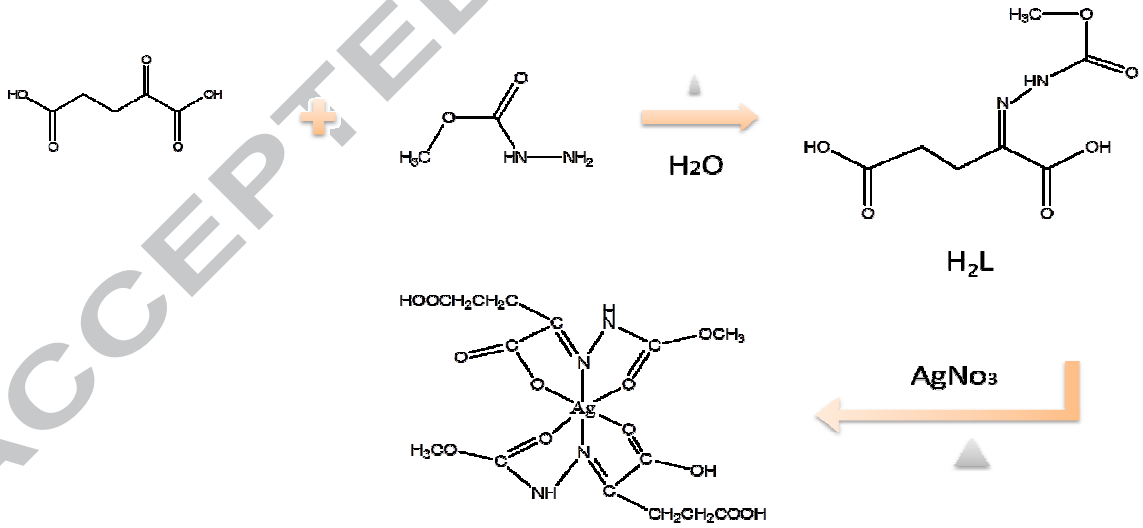

Scheme 1 Synthesis of Ligand (**H_2L**) and complex **[Ag(HL)(H_2L)]**

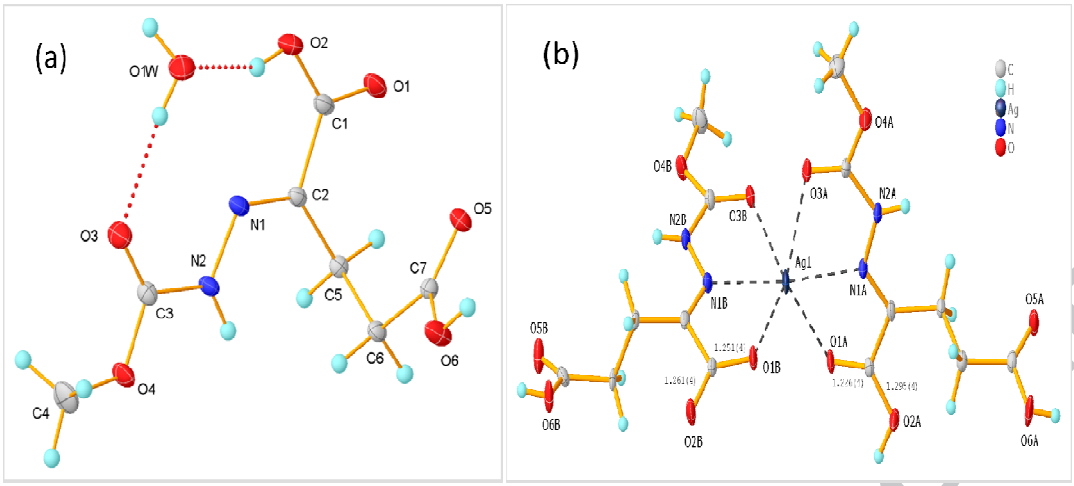

Fig. 1. X-ray molecular structure of **$H_2L.H_2O$ (a)** and **[Ag(HL)(H_2L)] (b)** with atom labelling scheme (thermal ellipsoids are plotted at 50% probability).

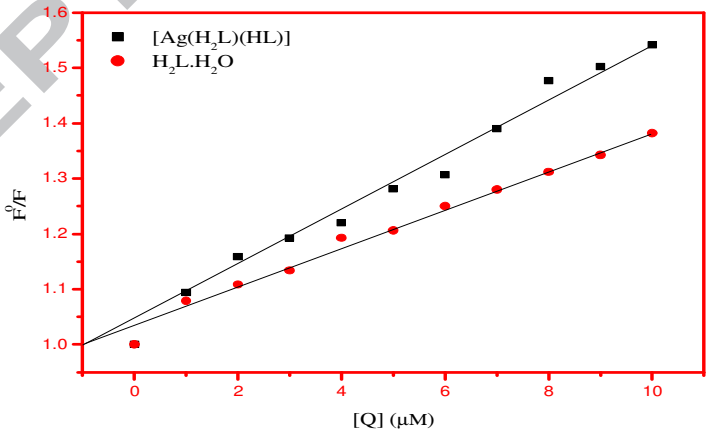

Fig. 2 Plot of F^0/F vs. [Q]

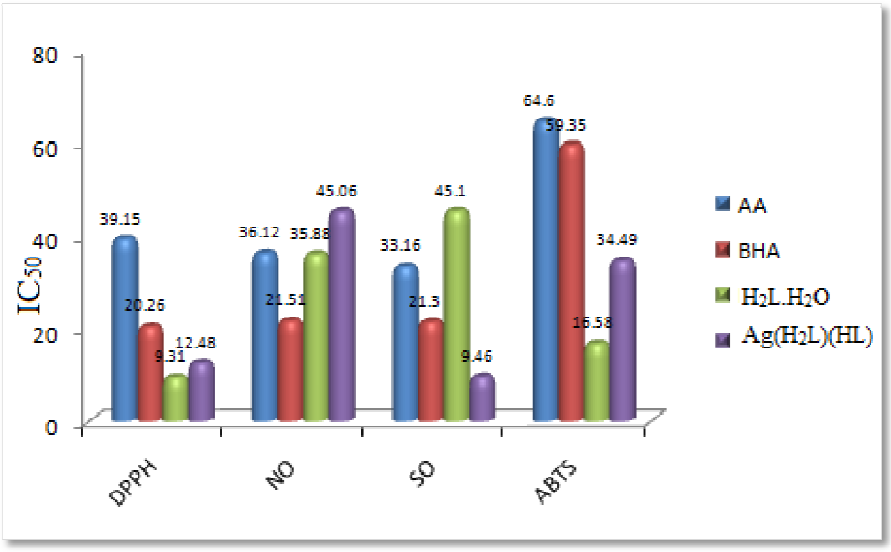

Fig. 3 Trends in inhibition of various radicals by ligand and complex along with the standard AA and BHA.

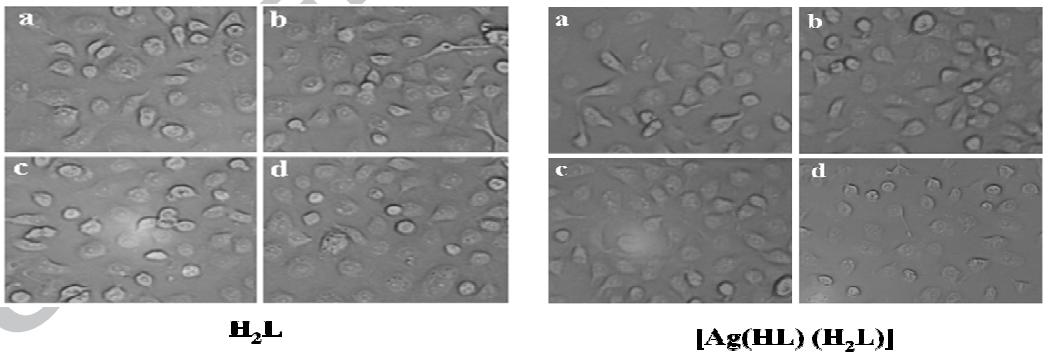

Fig.4 Microscopic images of MCF-7 cancer cells treated with compounds (ctrl (a), 10(b), 20(c), 40µM (d))

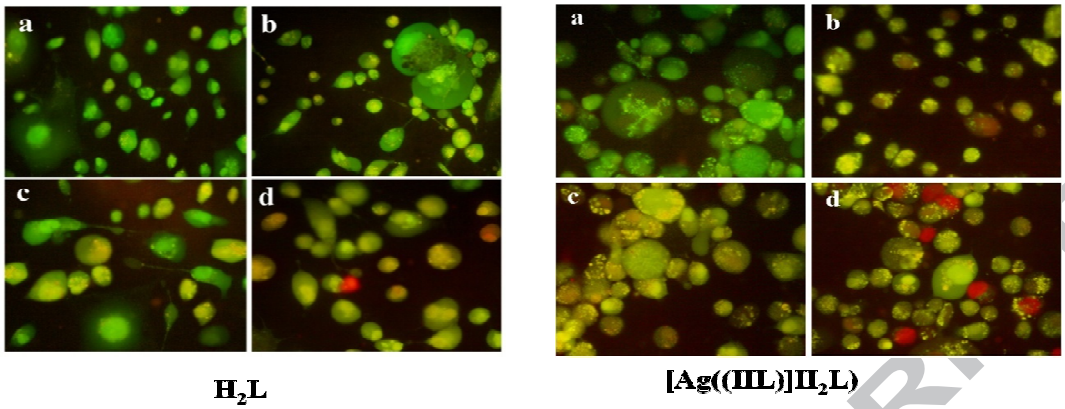

Fig. 5 AO/EtBr staining of MCF-7 cells using fluorescence microscopy after treatment with ligand and complex (0(a), 10(b), 20(c), 40 µM(d)) for 24 h.

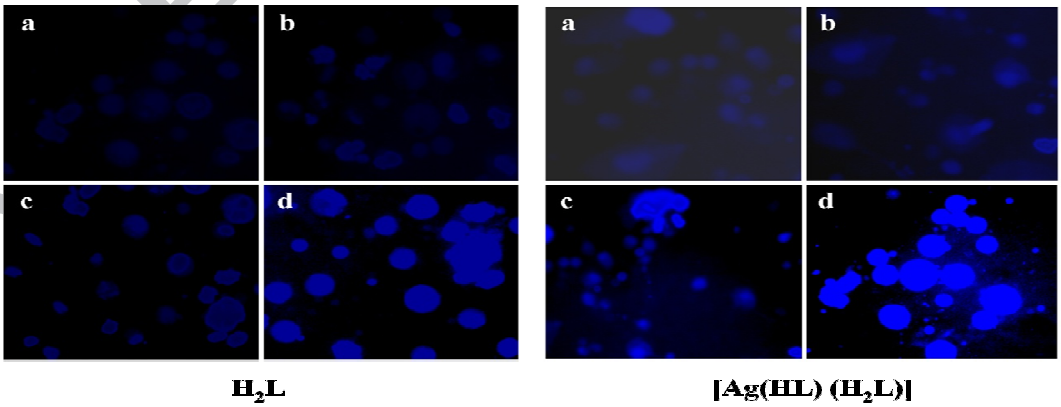

Fig. 6 Fluorescence microscopic images of MCF-7 cells after treatment with ligand and complex (0(a), 10(b), 20(c), 40μM (d)) for 24 h. Cells were stained with DAPI

Table 1

Crystal structure details of $H_2L.H_2O$ and $[Ag(H_2L)(HL)]$

Compound	$H_2L.H_2O$	$[Ag(HL)(H_2L)]$
Emprical Formula	$C_7H_{12}N_2O_7$	$C_{14}H_{19}AgN_4O_{12}$
$D_{calc.}$/ g cm^{-3}	1.533	1.886

Formula Weight	236.19	543.20
T/K	120(2)	120(2)
Crystal System	monoclinic	monoclinic
Space Group	$P2_1/c$	$P2_1/c$
a/Å	15.4170(3)	11.3309(4)
b/Å	5.69453(9)	12.1728(4)
c/Å	12.1388(3)	13.8242(5)
α/°	90	90
β/°	106.146(2)	92.035(3)
γ/°	90	90
V/Å^3	1023.66(4)	1905.56(11)
Z	4	4
μ/mm^{-1}	0.139	1.134
R_{int}	0.0402	0.0799
Crystal size/mm^3	0.79×0.35×0.14	0.41×0.14×0.13
Measured Refl.	51136	22881
Independent Refl.	3691	3940
Reflections Used	3214	3371
Restraints	0	36
GooF	1.040	1.083
Θ_{max}, Θ_{min}/°	32.844, 3.381	26.498, 2.457
N_{par}	151	288
Final R indexes [I>=2σ (I)]	R_1 = 0.0357, wR_2 = 0.0913	R_1 = 0.0423, wR_2 = 0.1054
Final R indexes [all data]	R_1 = 0.0436, wR_2 = 0.0967	R_1 = 0.0500, wR_2 = 0.1110
Largest diff. peak/hole / e Å^{-3}	0.460/-0.252	2.123/-1.185

Table 2

Antibacterial and antifungal activity of 100 µg/mL concentration of ligand, complex and metallic silver along with standard

Diameter of zone of inhibition in mm at 100 µg/ml and DMSO as control				
Organism	$H_2L.H_2O$	[Ag(HL)(H_2L)]	Ag	Std

Bacteria				
Bacillus substilis	12.2	14.9	10.2	34.25
Staphylococcus aureus	12.4	16.9	15.9	*14.8*
Stapylococcus albush	11.9	16.7	15.2	*28.5*
Salmonella paratyphi	10.7	18.5	15.6	28
Escherichia coli	12.1	17.9	16.8	22.9
Klebsella pneumonia	09.5	18.6	12.8	30.0
Fungi				
C.albicans	07.4	15.6	17.8	37.2
A.fumigates	07.2	07.3	16.9	41.5
A.niger	11.2	10.5	9.2	35.1

Graphical Abstract

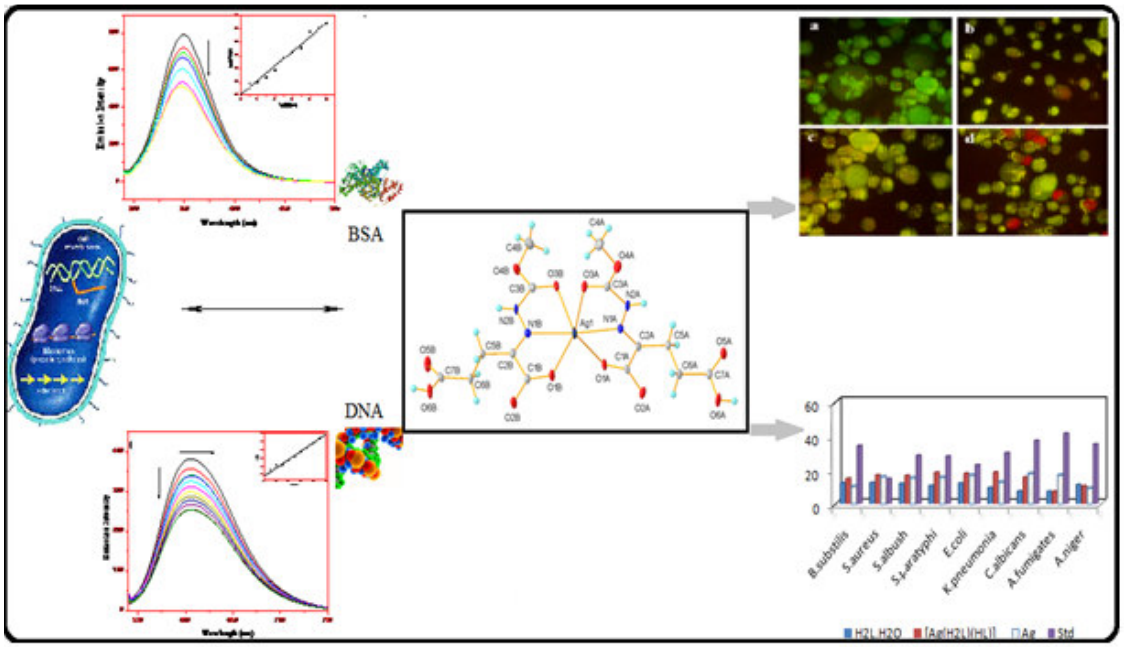

Antimicrobial and cytotoxic activities of silver are due to its ionised Ag+ form, and its ability to cause damage to cells by interacting with cell membrane protein and DNA. These effects have been visualised in our newly synthesised ligand and complex through BSA and CT-DNA binding studies. Silver sheets are produced by the decomposition of silver complex. Antibacterial and antifungal activities have been studied. With the increasing number of antibiotic strains of bacteria and fungi and low toxicity of silver, the use of silver as an antimicrobial agent is an exciting with a great deal in many fields.

Highlights

- New Silver(I) hydrazone Schiff base complex synthesised and characterised.
- Ligand and silver complex has the ability to interact with biomolecules (DNA,BSA).
- Excellent antimicrobial activity was observed for complex than free ligand.
- Preferential cytotoxicity observed for complex towards MCF-7 cancer cells and insignificant to normal breast cells.